WAVE PROCESSES AT MESO-, NANO-, AND MICROLEVELS

Optical Phenomena in Mesoscale Dielectric Spheres and Immersion Lenses Based on Janus Particles: A Review

B. S. Luk'yanchuk[a, *], **A. R. Bekirov**[a], **Z. B. Wang**[b], **I. V. Minin**[c, d], **O. V. Minin**[c, d], **and A. A. Fedyanin**[a]

[a] *Lomonosov Moscow State University, Moscow, 119992 Russia*
[b] *School of Electronic Engineering, Bangor University, Bangor LL57 1UT, UK*
[c] *Tomsk Polytechnic University, Tomsk, 634950 Russia*
[d] *Siberian State University of Geosystems and Technologies, Novosibirsk, 630108 Russia*
*e-mail: lukiyanchuk@nanolab.phys.msu.ru

Abstract—The mesoscale optical phenomena in dielectric spheres with a size parameter $q = 2\pi R/\lambda \sim 10$, where R/λ is the particle radius in incident wavelength units, have been considered. These phenomena make it possible to implement microscopy beyond the diffraction resolution limit. Another example of mesoscale optical phenomena is the field localization in immersion lenses based on Janus particles.

1. INTRODUCTION

Some interesting optical phenomena have recently been found in spherical dielectric particles with a size parameter $q = 2\pi R/\lambda \sim 10$, where R/λ is the particle radius in incident wavelength units. They include the photonic nanojet, Fano resonances of different orders, and optical anapole; these phenomena were considered in the first part of the review. In the second part we discuss in detail the effects of near-field localization of radiation as applied to microscopy beyond the diffraction resolution limit, as well as the specific features of field localization in immersion lenses based on Janus particles.

2. NANOSCOPY USING MICROSCOPIC DIELECTRIC PARTICLES

Considering the microscope as a device making it possible to view small objects with magnification, one should admit that such devices had been known long before the discovery of Zacharias Janssen and his father Hans in 1590 [1]. The direct participation of Zacharias Janssen in this finding belongs to the category of myths because the year of his birth was established to be specifically 1590. Meanwhile, even Seneca (4 BC−65 AD) wrote about the magnifying effect of a glass sphere, when looking through it as a text written in small letters. Another contender for the title of microscope inventor (in 1609) is Galileo; this invention was a kind of technical modification of telescope for him. The legend says that Galileo used a short-focus lens in order to improve the telescope and saw as a result an enlarged fly through his telescope. Fifty years later, Robert Hooke used a microscope to discover the cellular texture of biological structures and described the eye of a flea. Incidentally, Hooke used a glass sphere filled with water for illumination in his microscope. In 1674 Leeuwenhoek designed a short-focus microscope (with a lens size and a focal length of about 1 mm) having a magnification from 300 to 500, which allowed him to observe bacteria for the first time. Finally, in 1866, Ernst Abbe formulated the theory of limiting resolution (diffraction limit) of microscope, according to which light cannot be focused into a spot with a radius smaller than

$$r_D = \frac{\lambda}{2n \sin \theta}. \tag{1}$$

Here, λ is the light wavelength, $n\sin\theta$ is the numerical aperture, and n is the refractive index of the medium. For green light ($\lambda = 500$ nm) in vacuum, the resolution limit is 250 nm. In 1906 Zsigmondy developed the method of dark-field microscopy, and Synge proposed the concept of near-field optical microscope in 1928. Among the earlier theoretical achievements, we should note Euler's idea (1747) of eliminating chromatic aberrations. This idea was implemented by Aepinus and Tiedemann in the beginning of the next century (1805−1808).

An expression for the diffraction limit, similar to formula (1), can be derived from the Heisenberg uncertainty principle for the momentum and coordi-
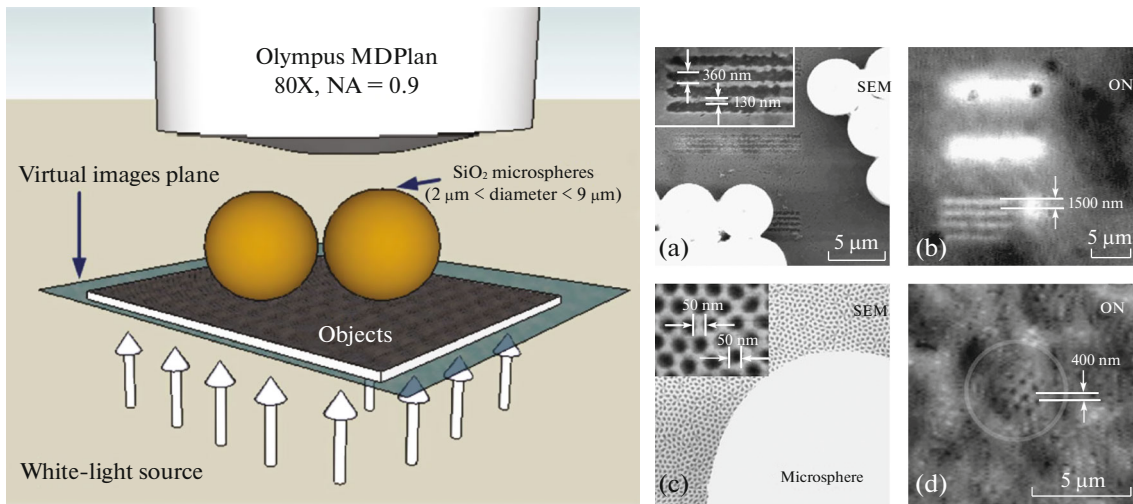
Fig. 1. (Color online) Schematic diagram of the nanoscope. Microspheres 2−9 μm in size are placed on different surfaces with nanostructures. These spheres collect information about the object near field and form virtual images, which are then viewed in a conventional objective. In panels (a) and (b) the object is a diffraction grating with a linewidth of 360 nm; the lines are spaced by 130 nm. (a) Scanning electron microscopy (SEM) image. (b) Image obtained in an optical nanoscope, in which lines are clearly resolved. The enlarged image in the top corresponds to a magnification factor of 4.17. (c) SEM image of the object and a microsphere. (d) Image viewed in an optical nanoscope. One can clearly see pores 50 nm in diameter, spaced by 50 nm [5].

nate: $\Delta x \Delta p \geq \hbar/2$. It also follows from the same Heisenberg principle that a field can be localized on scales smaller than the diffraction limit by providing fast damping of intensity in the perpendicular direction [2, 3]. This concept was implemented in the near-field optical microscope. It is noteworthy that, in the conventional statement of the microscopy problem, the case in hand is the localization of bright field against a dark background. In principle, one can put a question about the limit of dark field localization against a bright background. It turned out that the diffraction limit does not exist for a dark field: the darkness can be focused into an arbitrarily small dark spot [4].

An important discovery was made in 2011: it was experimentally demonstrated that a lens of micrometer size allows to resolve in white light nanostructures about 50 nm in size in a virtual image [5] (Fig. 1). Several mechanisms of this phenomenon have been proposed (see, e.g., [3–9]). Localization of magnetic fields is related to the currents arising during the electric charge motion. The magnetic field at the center of a circular turn of radius R with a current I is given by the Biot−Savart law: $B = \mu_0 I/2R$. It follows from this formula that the magnetic induction may be arbitrarily large for an arbitrarily small turn [4].

Applying the rules of geometric optics to a transparent sphere, one can easily find the position of the virtual image plane, $z_{vi} = nR/(2-n)$, and the corresponding magnification: $M = n/(2-n)$. In these formulas n is the refractive index and R is the sphere radius. One can see that the above formulas have a limited range of applicability: they are invalid at $n \to 2$, because in this case $M \to \infty$, and the particle sizes are

on the order of several light wavelengths λ, whereas the formulas of geometric optics are valid when $R \gg \lambda$ [10]. To describe theoretically the experiments performed in [5], one must consider the virtual image in the framework of the wave theory. If the solution to the wave equation in some plane (for example, $z = 0$) is known, the field in the entire space $(z > 0)$ can easily be determined. To this end, it is sufficient to perform the inverse Fourier transform:

$$A(x,y,z)$$
$$= \left(\frac{1}{2\pi k_0}\right)^2 \int_{-\infty}^{\infty}\int_{-\infty}^{\infty} A_k \exp\left[ik_x x + ik_y y + ik_z z\right] dk_x dk_y, \quad (2)$$
$$A_k = \int_{-\infty}^{\infty}\int_{-\infty}^{\infty} A(x,y,0)\exp\left[-ik_x x - ik_y y\right] k_0^2 dx dy.$$

To determine the virtual-image parameters, one must calculate the Fourier transform for the backward propagation of light from the source, i.e., in the space $z < 0$. In this case, the range of integration is limited in the wave-vector space: $k_x^2 + k_y^2 \leq k_0^2$ [11, 12] ($k_0 = 2\pi/\lambda$ is the wave vector of incident light):

$$A_{im}(x,y,z)$$
$$= \left(\frac{1}{2\pi k_0}\right)^2 \iint_{k_x^2 + k_y^2 \leq k_0^2} A_k^* e^{-i(k_x x + k_y y + k_z z)} dk_x dk_y, \quad (3)$$

where the asterisk means complex conjugation. If the field A in formula (2) is the field of a point source in free space, formula (3) yields the distribution of field A_{im}, which is maximum at the point of source location,
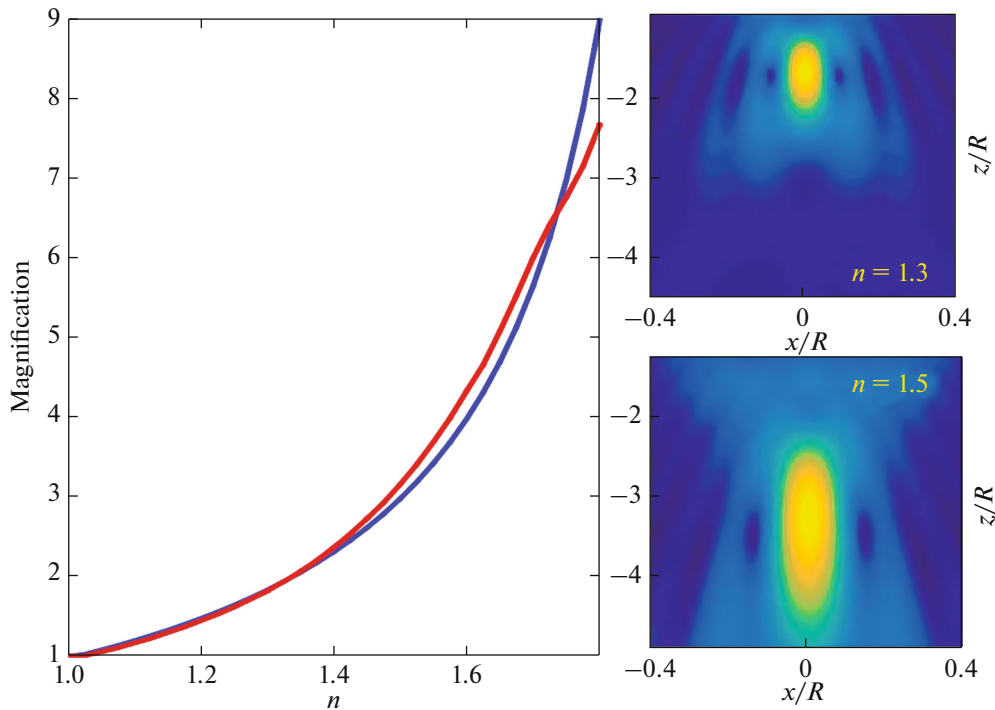
Fig. 2. (Color online) Comparison of the results obtained in terms of the geometric (blue line) and wave (red line) optics for a size parameter $q = 100$. The range of integration in integral (2) is a square with a side of $2R$ and a center located on the z axis at the point $z = 1.05R$. With an increase in the refractive index the sizes of the virtual-image localization domain increase as well. Blurred virtual images of a point source, viewed with the aid of spheres with refractive indices $n = 1.3$ and 1.5, are shown on the right [11].

with a half-width described by formula (1) [12]. If there is a dielectric sphere of radius R between the point source and the aperture of the optical device, the position of the local maximum of field (3) coincides with that given by the formula of geometric optics: $nR/(2 - n)$ [11, 12]. Note that, for a point source $\mathbf{E}^i$ in form of a derivative with respect to the Green's function $G = \dfrac{\exp[ik\,|\mathbf{r} - \mathbf{r}_0|]}{k\,|\mathbf{r} - \mathbf{r}_0|}$, as well as for any sources that do not obey the condition $\operatorname{div}\mathbf{E}^i = 0$, longitudinal modes must be taken into account when expanding fields in eigenfunctions [11]. This is the difference from the standard procedure in the Mie theory [13], where longitudinal modes do not play any role. The formulas of the wave theory describing the distribution of fields from different sources were reported in [11, 12].

Figure 2 shows a dependence of the virtual-image magnification factor M in a dielectric sphere with a size parameter $q = k_0 R = 100$ on the relative refractive index. The point object is located on the sphere surface. The plot also shows magnification in the limit of geometric optics. Despite the fact that the formal requirements of geometric optics are satisfied in the above example ($q \gg 1$), the difference between the two dependences, as expected, increases while the refractive index approaches 2.

Image blurring can be observed in the insets to Fig. 2. The reason is that the rays forming the virtual image are concentrated in some limited angular range: $\theta < \pi/2$. For this reason the "blurring" is consistent with the classical concepts. From the point of view of the "wave" optics, the blurring occurs because a finite number of image-forming modes are considered. In the Mie theory the number of modes making a significant contribution to the field formation is estimated by the formula $q + 4.3\,q^{1/3} + 1$ [14]. The virtual-image field contains one or several maxima. Figure 3a shows the virtual image of a point source located at the boundary of a sphere with the parameters $q = 24$, $n = 1.32$, and the number of modes $L_{\max} = 37$. Based on this figure, one can also determine the position of the field maximum. If one places a point source at this point and views its image in the absence of the sphere, this image is also blurred, depending on the number of the modes presenting the source (see Figs. 3b, 3c). Image localization is observed for a source with a large number of modes. If a source is placed inside the sphere, the number of modes $q + 4.3\,q^{1/3} + 1$ is sufficient to form an image with a half-width on the order of $\lambda/2$. For a source located beyond the sphere, this number of modes is insufficient for image localization.
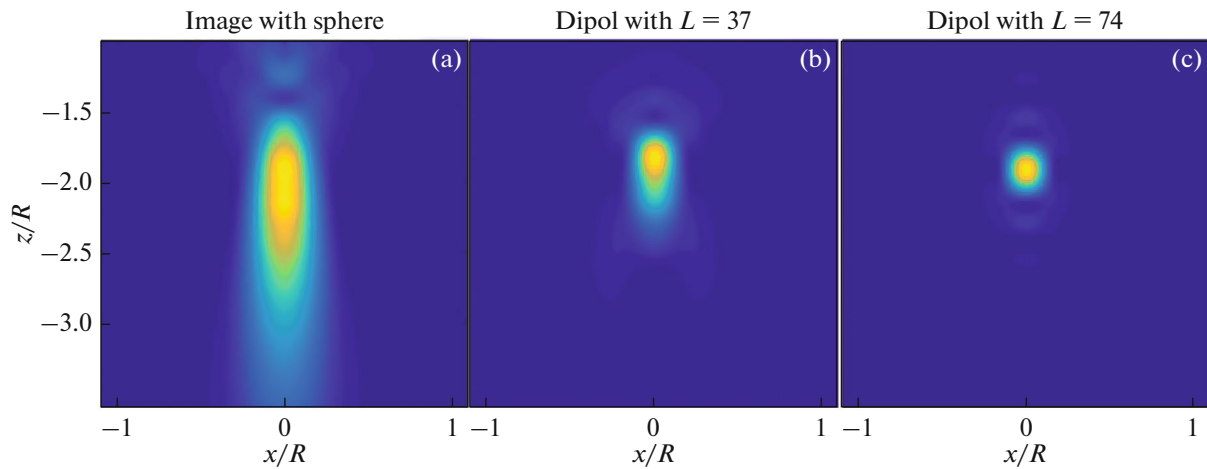
Fig. 3. (Color online) Comparison of the field of image (3) in the cases of (a) virtual image of a point source located on a sphere; (b) a point source without a sphere, with expansion in 37 modes; and (c) a point source without a sphere, with expansion in 74 modes.

The blurring effect can be attenuated if several local maxima are observed in the image field. In this case a resolution as high as $\lambda/4$ can be obtained [15]. This effect was related in [15] to the excitation of whispering-gallery waves. However, no resonant effects corresponding to the excitation of these waves were observed in experiments.

If we consider some distributed structure (e.g., an array of slits in a metal screen) instead of a point source, the summation of "broad" fields may lead to interference effects, which increase resolution. The virtual image of such slits in dielectric spheres was studied experimentally in many works; see, e.g., [5, 8, 16−19]. This increase in resolution is also observed in the wave theory of the virtual image [11, 12]. Figure 4 shows the image calculated for four slits; in this case, one can speak about resolution on the order of $\lambda/4$. This calculation was performed considering the reflection from the metal screen, which affects the image contrast [20−26]. An increase in resolution is observed in this case in a wide range of values of size parameter q.

In principle, the surface a particle lies on affects the resolution. As an example we will consider an ideally conducting surface. For example, there are real and reflected images of a particle lying on a conducting surface. Scattering is described in this case by the summation of the spherical waves emanating from the real and reflected particles [27]. The presence of two centers of emanating waves leads to doubling of the number of modes available for image construction. In this case the point source can be expanded in two bases, which gives rise to an image with extremely small blurring, as shown in Fig. 3c (although the number of modes considered in each basis is $L = 37$).

As a physical realization of a point source, we can consider a small Rayleigh particle exposed to laser radiation. Figure 5 shows the calculation result for a gold nanoparticle 100 nm in diameter, located near the surface of an ideal conductor and viewed using a SiO_2 sphere: $q_1 = 23$, $n_1 = 1.48$, $q_2 = 0.5$, $n_2 = 3$. In this case small particle 2 is a field source similar to a dipole. The calculated image is similar to that obtained for a point source.

The construction of a virtual image in classical optics has been studied since the time of Galileo and his telescope, where a concave diverging lens formed an enlarged virtual image of object. For particles with sizes on the order of few light wavelengths λ, the geometrical optics approximation is not valid, and one must use the wave theory of virtual image. For random reasons this theory turned out to be a blank spot on the map of classical optics. Experimental and theoretical studies show that a virtual image in micrometer-sized particles makes it possible to resolve the structure below the diffraction limit (for example, at a level of $\lambda/6$ or even smaller). The theoretical limit of resolution depends also on the surface roughness, coherence, and exact field distribution inside the slit. Experiments demonstrate resolution at a level of $\lambda/8$ in white light (structures about 50 nm in size were resolved in [5]). A higher resolution can be obtained by decorating the surface sphere with metal concentric rings [28]. This approach combines the photonics and plasmonics concepts. The theoretical limit of resolution in optics, according to the theory of information [29], is related to the signal-to-noise ratio (SNR). The resolution corresponding to SNR $\sim 10^{-6}$ may be as high as $\lambda/100$. The use of the technique based on super-oscillations [30] makes it possible to reach a resolution on the order of $\lambda/1000$. The experimentally implemented value of optical resolution is $\lambda/800$ [31]. Thus, the Abbe criterion (1) is in fact far from the real physical limit for the far-field optical resolution.

The use of micrometer-sized lenses allows one to obtain super resolution even in a school microscope.
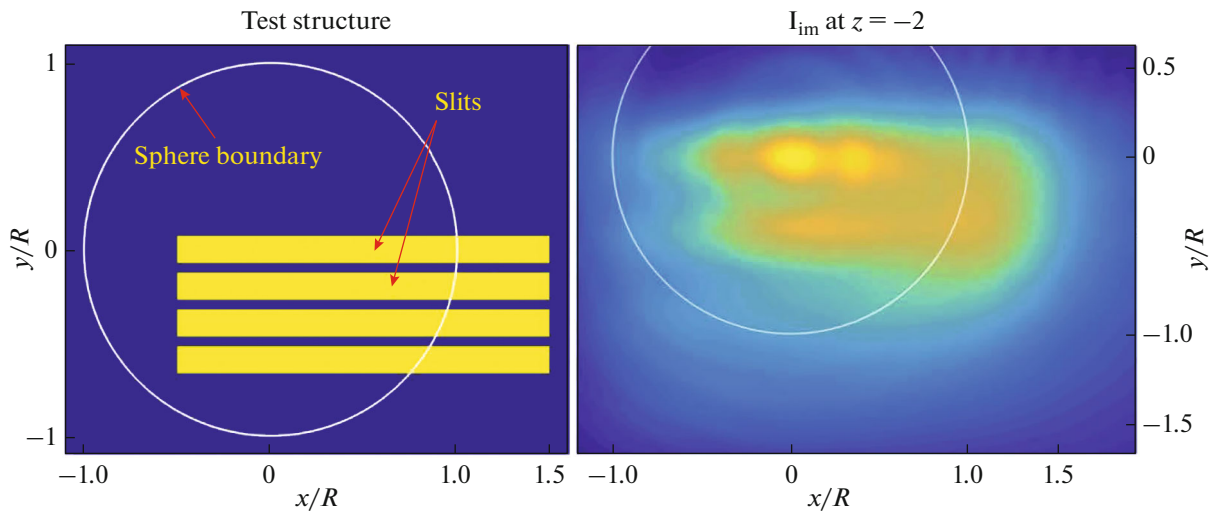
Fig. 4. (Color online) Calculated virtual image of four neighboring slits. The geometry in the left image is similar to that in [5], strips 360 nm wide are spaced by 130 nm, the wavelength is 600 nm, and the microsphere diameter is 4.96 μm. The field of view at $z/R = -2$ makes it possible to see only two bands, but with a large magnification. On the right panel only two strips out of four can be seen. The visibility of four strips in the experiment illustrated in Fig. 1b is likely due to the fact that strips are located inside an array of spheres, in contrast to our consideration with one isolated sphere. Note that the field polarization in a slit also affects the resolution [26].

The most impressive breakthrough in this field was the possibility of designing lenses with a super resolution in the form of metamaterials, using the cluster assembly method [3, 32]. Such lenses make it possible to see 45-nm structures in an ordinary school microscope (Fig. 6).

Despite the fact that the physical mechanisms of nanoscopy with the aid of dielectric particles are still being studied [33, 34], some key aspects of this technique can be selected. Since the time of Rayleigh [35] it was believed that the fundamental limitation for the resolution in classical optics is related to the fast damping of evanescent waves, carrying information about the high harmonics of an image. However, about a dozen of methods bypassing this limitation were proposed in the last century, including near-field microscopy [2, 36], lenses with a negative refractive index [37, 38], STED-fluorescent microscopy (awarded a Nobel prize) [39, 40], optical super-oscillatory lenses [41], scanning laser confocal microscopy [42], etc. [3].

Several possible mechanisms of nanoscopy using dielectric spherical particles have been described in the literature. Focusing of radially polarized light is known to give rise to a beam of longitudinally polarized light beyond the diffraction limit [43, 44]. It was suggested in [9] that a dielectric sphere forms such longitudinally polarized light under certain conditions. The concept of this mechanism is clarified in Fig. 7. If a radially polarized point dipole is placed near the sphere surface, the rays emerging from this point source, in the geometric optics approximation, pass through the sphere only at the angles smaller than the total internal reflection angle: $\alpha < \alpha_{cr} = \arcsin(1/n)$ (n is the refractive index).

The radially polarized rays at the output of the sphere make an angle β with the axis; this angle is given by the formula

$$\beta = \arcsin\left(n \sin\alpha\right) - 2\alpha. \qquad (4)$$
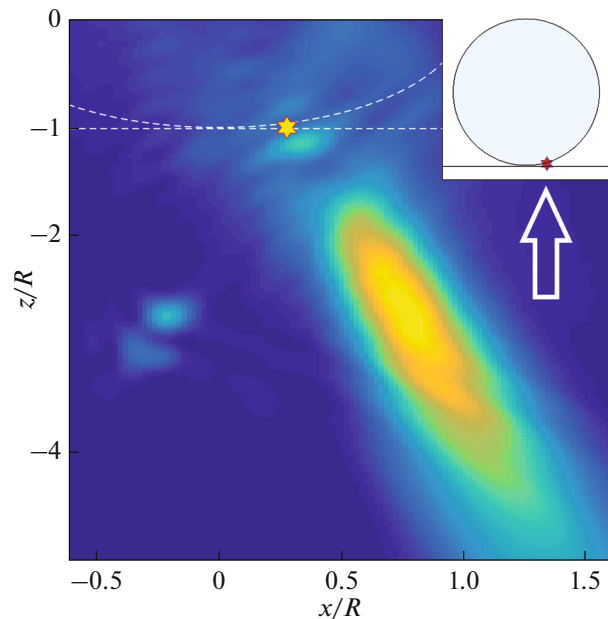

Fig. 5. (Color online) Two particles located on an ideally conducting surface. The scattering from a small spherical particle (denoted by an arrow and an enlarged red star in the inset) imitates a point source. In the pattern with a virtual image a sphere on the substrate is shown by a dashed line, and the point source is presented as an enlarged yellow star.
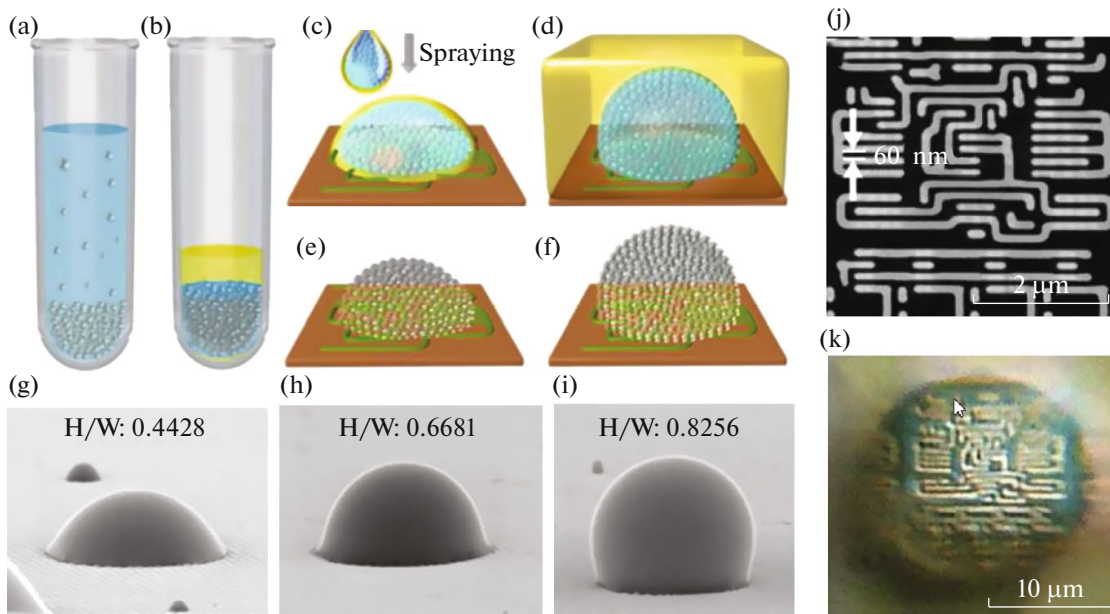
Fig. 6. (Color online) Schematics of the formation of a lens from a metamaterial, collected by cluster assembly. (a) Anatase nanoparticles (15-nm TiO_2) are centrifuged to form a dense precipitate; (b) the liquid above the precipitate is replaced with a mixture of organic solvents (hexane and tetrachloroethylene), which form a "nanofluid fraction" (NFF) of TiO_2; (c) to from a hemispherical metamaterial, this NFF is deposited as a "drop" directly on the sample surface; (d) to from a hemispherical metamaterial, this drop is coated by a thin layer of a mixture of organic solvents; (e, f) after the solvent evaporation the "drop" undergoes a phase transition with the formation of a more closely packed metamaterial; (g–i) fabricated lenses with different height-to-diameter ratios; (j) SEM image of a part of an integrated circuit with 60-nm elements; and (k) a view of the same integrated circuit in an optical microscope with a 15-μm metamaterial lens [32].
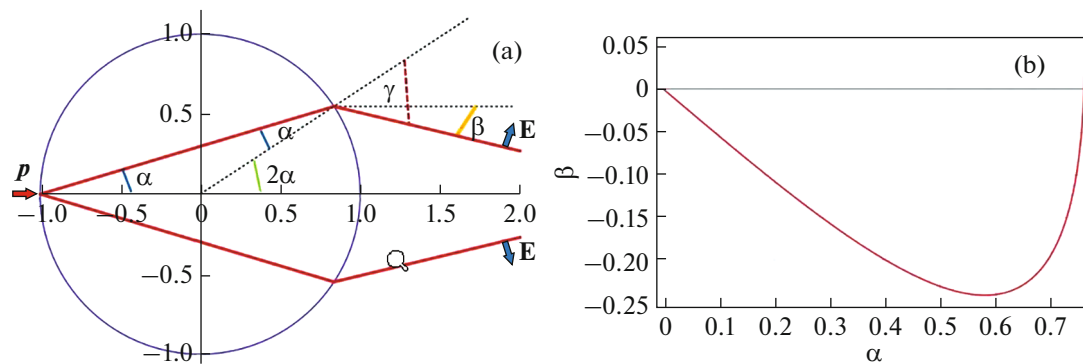

Fig. 7. (Color online) (a) The point light source is a radially polarized dipole p, located near the surface of a sphere. A ray from this source propagates at an angle α, smaller than the total internal reflection angle. At the output of the sphere this ray is refracted at an angle $\gamma = \arcsin(n\sin\alpha)$ and propagates at an angle β with respect to the axis [9]. (b) Example of a solution to Eq. (4) at $n = 1.45$.

This concept was developed further in [45, 46]. In principle, this approach can be implemented using illumination of the sphere by a source of radially or circularly polarized light. The calculations performed in [47] showed that radially polarized light forms a multifocal structure with oscillating electric field intensity at the particle output, while azimuthally polarized light forms a similar structure with oscillating magnetic field intensity (Fig. 8). This is a beam of azimuthally polarized light. A magnetic nanojet with a multifocal longitudinal polarization of magnetic field is formed at the sphere output. Similar field modulations are observed in the case of waveguide propagation of a magnetic mode in a chain of silicon nanocylinders [48]. Far from the sphere the Bessel beam "recovers" the value of the initial longitudinal magnetic field.

Another mechanism of resolution beyond the diffraction limit was proposed in [8]; it implies an adiabatic lens using a geometrically conformal surface to
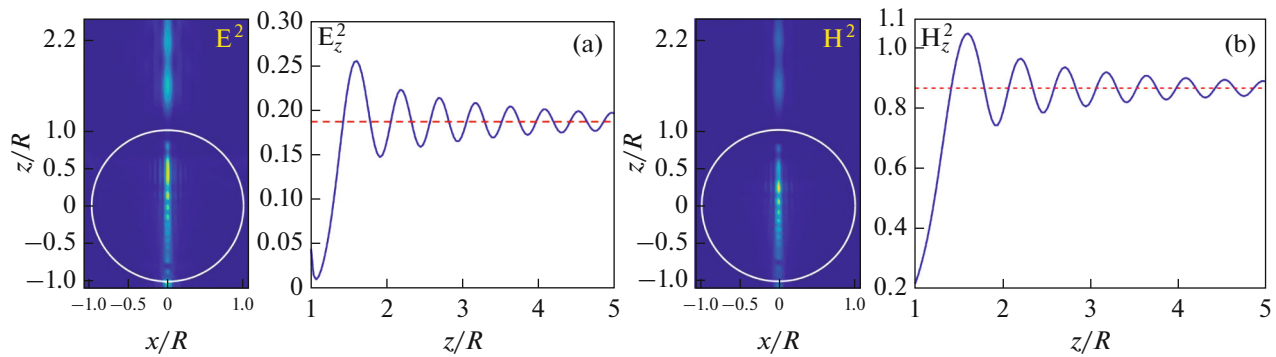
Fig. 8. (Color online) (a) Distribution of $\mathbf{E}^2$ in the plane $y = 0$. The E_z component of electric field along the z axis is shown on the left. The beam and sphere parameters are as follows: $k_z = 60.5$, $n = 1.5$, and $q = 30$. The dotted line indicates the longitudinal component of incident electric field. (b) Distribution of $\mathbf{H}^2$ in the plane $y = 0$. The H_z component of magnetic field along the axis z is shown on the right. The beam and sphere parameters are as follows: $k_z = 0.5$, $n = 1.5$, and $q = 30$. The longitudinal magnetic component of incident field is denoted by a dashed line.

provide the interference of slowly decompressed electromagnetic waves in the far field for image formation. Decompression satisfies the adiabatic condition, due to which the far and near fields are matched, and the far-field optical system can directly project the image of near-field elements.

The concept of this mechanism is clarified in Fig. 9 for the case of a metal sphere located above a metal surface. When a surface plasmon propagates above metal surface 2, its frequency increases with a decrease in the gap between the sphere surface 1 and the horizontal surface. Correspondingly, the local wavelength decreases. During further propagation of the surface plasmon above the sphere surface, its frequency decreases while moving away from the gap, and the corresponding wavelength increases. As a result, the optical information about the small image near the particle south pole is transferred with some magnification onto the surface near the north pole. The corresponding magnification may be as high as 20, due to which an image resolution less than 50 nm in the visible range can be obtained. The advantages of this mechanism are obvious; however, it is unclear how to apply this concept to the case of a dielectric particle located above a dielectric structured surface.

The third mechanism appeals to the theory of super oscillations [49]. A high degree of localization of electric and magnetic fields can be provided in the domain of wave-field singularities. In the review [50] this mechanism was discussed in the context of generation of giant magnetic fields [4]. In this case the super resolution is due to the possibility of localizing the "magnetic light" [51] beyond the diffraction limit.

Concerning the super resolution of a lens formed by an ensemble of nanoparticles (see Fig. 6), this effect may be related to the specificity of light transmission through a photonic crystal [52]. This behavior agrees with the results of the numerical simulation of [53],

where the Maxwell equations were solved using the CST Microwave Studio package for the transmission of a plane electromagnetic wave with a wavelength $\lambda = 550$ nm through a layer of closely packed 15-nm TiO_2 nanoparticles (the anatase refractive index is $n = 2.55$), separated by air gaps (Fig. 10). These calculations demonstrate that an electromagnetic wave passes through seven layers of nanoparticles and forms
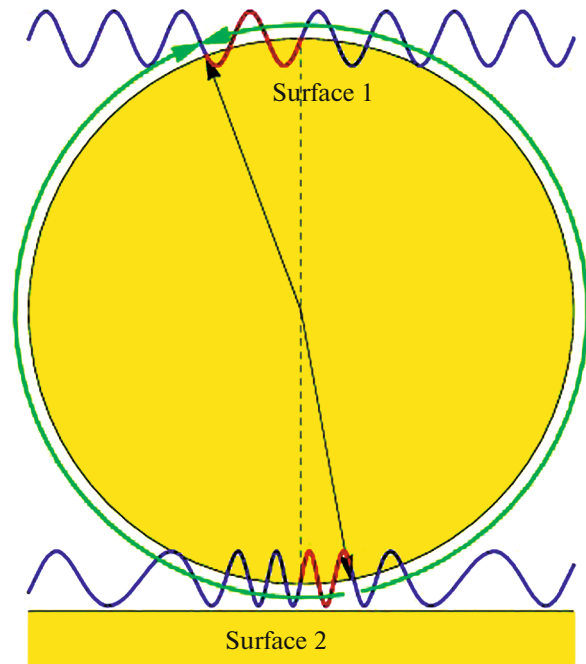

Fig. 9. (Color online) Schematic diagram of surface electromagnetic waves (blue lines) near the south and north sides of sphere. The wave in the range of one wavelength is shown red. This mechanism provides a resolution on the order of 50 nm in the visible range [8].
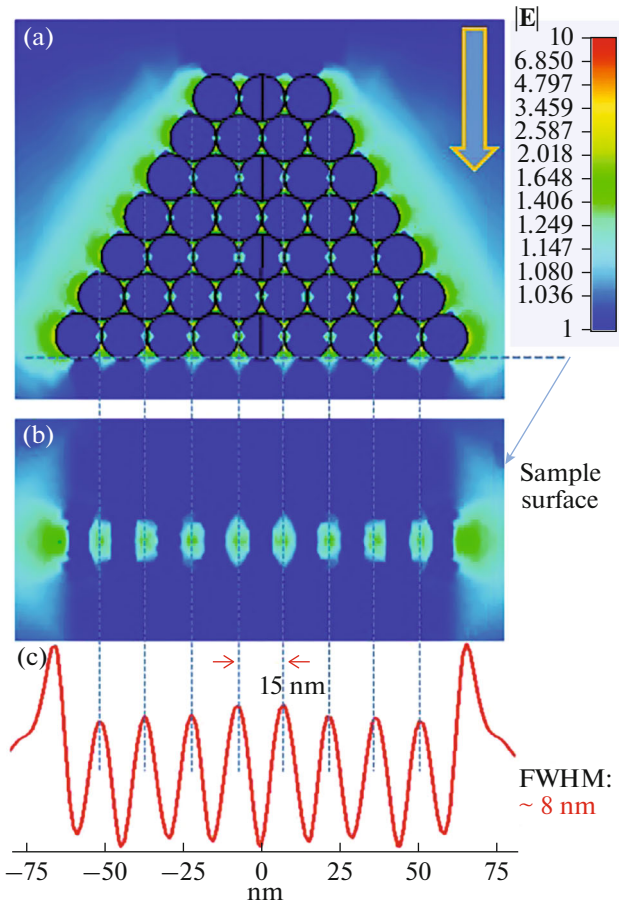
Fig. 10. (Color online) Transmission of a plane electromagnetic wave through a pyramid formed by 15-nm TiO$_2$ nanoparticles [53].

an intensity distribution with a period of 15 nm at the output.

The transmission of a signal from two-point sources (spaced by 45 nm) through a 500-nm layer of a homogeneous medium and a medium consisting of closely packed 15-nm TiO$_2$ nanoparticles (Fig. 11) was also simulated in [53]. Fast damping of the evanescent wave was observed for the homogeneous medium, which led to image blurring, in agreement with the diffraction limit. At the same time, transformation of the evanescent wave into a propagating wave with a period of 160 nm was observed for the medium consisting of closely packed TiO$_2$ particles. In this case, a signal transmitted through the medium makes it possible to distinguish between two sources.

Finally, there is a possibility of increasing resolution using numerical methods of image processing [54]. The fast development of dielectric micro spherical lens nanoscopy [32] gives grounds to believe that optical observation of viruses in a school microscope will become possible even in the near future.

3. IMMERSION LENSES BASED ON JANUS PARTICLES

A transparent dielectric sphere with a diameter of more than three wavelengths of the light incident on it can play the role of either a focusing lens in the photonic-jet mode or a cavity concentrating energy in a whispering-gallery wave in the near-wall region [6]. A transition from the photonic-jet mode to the cavity mode with whispering-gallery waves occurs with a change in the sphere size or the radiation wavelength. Both phenomena are described excellently within the Mie theory (see, e.g., [4]). New phenomena arise in Janus particles, i.e., particles with a removed segment of a sphere or a cylinder [55, 56]. This is a typical design of an immersion lens [57, 58]. It is known that the parameters of a photonic jet emerging from a hemisphere or a half-cylinder may differ significantly from the parameters of a jet formed by an integer sphere [59] or an integer cylinder [60]. Optimizing the thickness of the removed segment, one can form a highly localized field distribution [61]. This effect in cylinders can be used in contact optical lithography with a super resolution in the line thickness.

The main concept for this study is that a Janus particle [62] exhibits a combination of the photonic-jet and whispering-gallery wave effects [61]. The focusing effect due to the photonic jet can be clarified qualitatively using the ray-tracing method [63] (Fig. 12). The following form of caustic can be obtained for a truncated sphere:

$$z_c = 1 - h - \frac{\sec\beta}{n} \frac{\left(1 - n^2\sin^2\beta\right)^{3/2}}{\cos\varphi - \sqrt{n^2 - \sin^2\varphi}}$$
$$\times \Bigg(\cos\varphi\sqrt{n^2 - \sin^2\varphi} + (1 - h + \cos\varphi) \qquad (5)$$
$$\times \sec^2\beta\left(\cos\varphi - \sqrt{n^2 - \sin^2\varphi}\right)$$
$$+ \sin\varphi\sqrt{n^2 - \sin^2\varphi}\tan\beta \Bigg),$$

$$y_c = y_{out} - (z_c - 1 + h)\tan\gamma,$$
$$\gamma = \arcsin\left[n\sin(\varphi - \theta)\right],$$
$$y_{out} = \sin\varphi - (1 - h + \cos\varphi)\tan(\varphi - \theta), \qquad (6)$$
$$\beta = \varphi - \theta, \quad \theta = \arcsin\left(\frac{\sin\varphi}{n}\right).$$

Here, h is the truncation height normalized to the particle radius R, φ is the angle of incidence, and θ is the angle of refraction. The singularity point of a Janus particle is located at a distance of

$$z_f = z_c\big|_{\varphi \to 0} = 1 - \frac{2}{n} + \frac{1}{n-1} + h\left(\frac{1}{n} - 1\right). \qquad (7)$$

The main effect with a Janus particle is related to the change in the focal length of a truncated particle in comparison with the initial solid sphere. For example, a sphere with $n = 1.33$ has a focal point located at a dis-
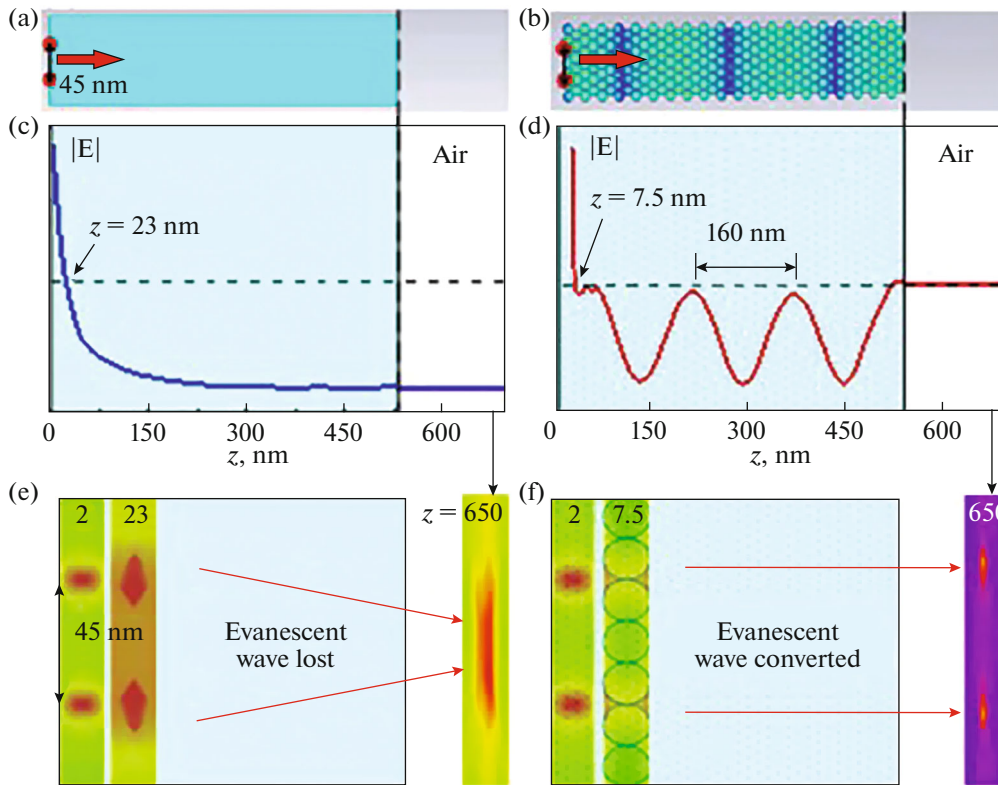
Fig. 11. (Color online) (a) Homogeneous medium consisting of anatase TiO_2. (b) Metamaterial composed of closely packed 15-nm anatase nanoparticles. (c) The amplitude of mean electric field as a function of the distance from point incoherent sources with transverse electric polarization. The amplitude decays exponentially at a distance of 50 nm. (d) The damping waves propagating in the metamaterial interact with TiO_2 particles and are transformed into propagating waves leaving for the far field. (e, f) Image from two point sources, spaced by 45 nm, formed at a length of 650 nm (far field beyond the 500-nm-thick sample) after passing through the homogeneous medium (e) and metamaterial (f) [53].
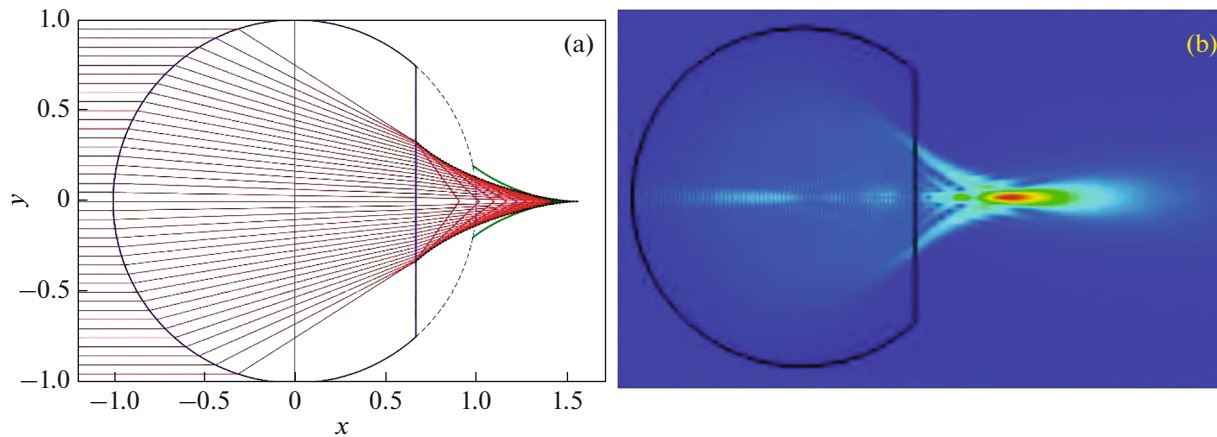

Fig. 12. (Color online) (a) Rays emerging from the sphere after the second refraction by an angle γ obey Snell's law: $\sin\gamma = n \sin(\varphi - \theta)$. The focused-beam boundary is a caustic for a truncated sphere with $h = 1 - 1/n$ and $n = 1.5$. The solid green line is the caustic for a spherical particle with the same refractive index. (b) Result of exact solution of the Maxwell equation for the same values of parameters and $q = 2\pi R/\lambda = 100$.

tance of $z_f = 2.015$. After removing a small segment with $h = 0.07$, the thus obtained Janus particle has a focal point with $z_f = 2.509$; i.e., the truncation yields an elongated focus. Approximation by the ray-tracing method

yields a qualitatively correct description of the focusing properties of a transparent dielectric Janus sphere.

The truncated particle is a solid immersion lens (SIL), which can be used to overcome the diffraction
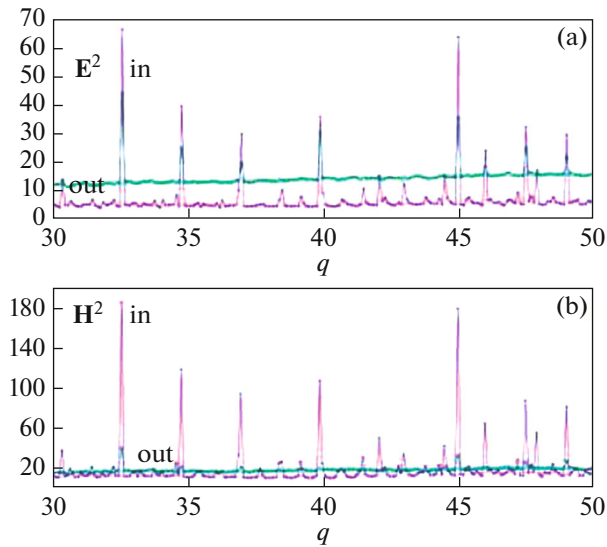
Fig. 13. (Color online) Maximum internal (pink) and external (green) (a) electric field strength $\mathbf{E}^2$ and (b) magnetic field strength $\mathbf{H}^2$ for a cylinder with a fixed truncation parameter $h = 0.02$. The size parameter $q = 32.5$ corresponds to the cylinder radius $R \approx 5\lambda$ [61].

limit [64]. Note that the physical principles of operation of a truncated spherical SIL, characterized by aberration-free focusing (known also as the Weierstrass SIL) are based on the compression of emitted light into a small numerical aperture with a decrease in the angle of refraction of transmitted light, counted from the optical axis. This occurs when the sphere is truncated to a thickness $h = r(1 + 1/n)$, where r is the sphere radius and h corresponds to the aplanatic focus (see [65] (p. 253) and [62]). Such SILs were used in optical microscopy and photolithography [64]. An analysis of a photonic nanojet from a particle with a truncated spherical surface shows that the maximum intensity in the focus is lower than that for a spherical particle, but the effective focal length may be larger [61].

A numerical solution of the Maxwell equations for a Janus particle [61] shows a number of interesting features in the scattered-light intensity distribution. For example, at a fixed truncation $h = $ const, there are sharp resonances in the dependences of electric and magnetic field intensities on the size parameter (Fig. 13). For example, four sharp resonances can be seen in the range of variation in q from 35 to 45. Approximately the same resonance density is observed for high Fano resonances (see Fig. 4b in [4]).

With a change in the truncation thickness h (at fixed values of other parameters) one can observe a narrow resonance for the TM mode when the $\mathbf{H}$ vector of the incident plane wave lies in the x–y plane of truncated element of the sphere (Fig. 14a). A bright "diamond" arises in the sphere at the point of resonant truncation (Fig. 14b). The photonic-jet shape does not qualitatively change in this case (Fig. 14c). However, hot points with maximum intensity arise on the flat surface of the truncated element (Fig. 14d).

The whispering-gallery waves in a sphere are known to be due to the energy localization near the particle surface [66, 67] because of the total internal reflection of rays incident on the surface at small angles. However, the total internal reflection is absent on a curved surface, and the energy is partially leaked out beyond the particle. For this reason it is difficult to obtain a high Q factor for small spherical and dielectric cavities. Large Q factors ($Q > 10^6$) are obtained for only large spheres with a size parameter $q > 10^3$ [68, 69]. The Q factor of small spherical cavities can be increased using the interference method, which is based on the resonances caused by bound states in the continuum [70, 71].

The photonic jet effects for spherical and cylindrical particles were discussed in many studies (see, e.g., review [6] and the references therein). In the case of a cylinder with a radius R, the fields excited by an incident electromagnetic wave with a magnetic component directed along the cylinder axis are described by simple formulas [13, 72]. The scattered fields, denoted by the superscript s, are presented in cylindrical coordinates (r, φ, z) by expansions in Hankel functions
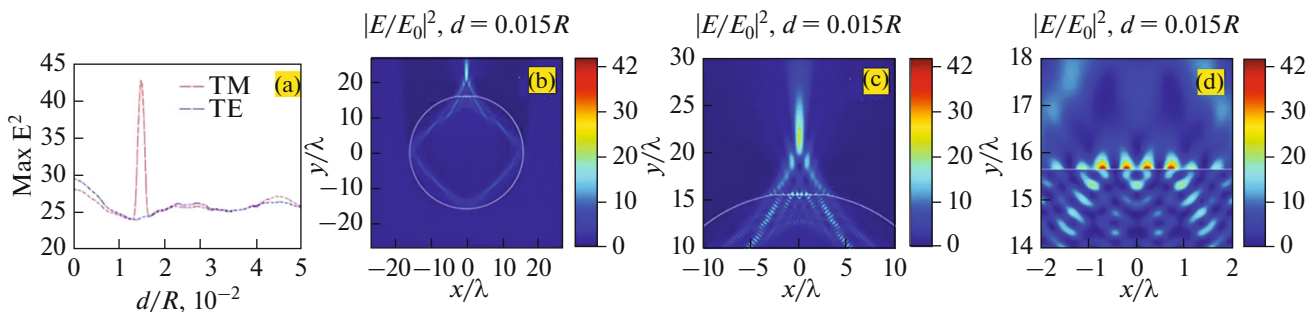

Fig. 14. (Color online) (a) Resonant effect for field amplification in a truncated cylinder, depending on the truncated-element thickness; refractive index $n = 1.5$, $q = 2\pi R/\lambda = 100$. The resonance is observed for only the TM mode and is not observed for the TE mode. (b–d) Intensity distributions at the resonant truncation value $h = d/R = 0.015$ for different magnifications [61].
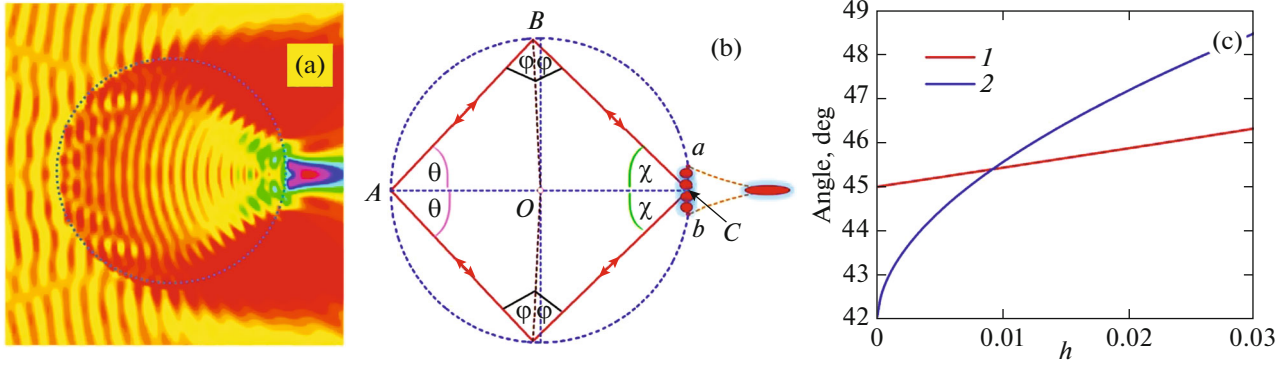
Fig. 15. (Color online) (a) Intensity distribution $I = |\mathbf{E}|^2$ in the cross section of a cylinder with a refractive index $n = 1.5$ and size parameter $q = 10$, according to formulas (8)−(15). (b) The ray path in a Janus particle in the case of ray incidence on a planar surface ab at a total internal reflection angle χ. (c) Resonant angle χ (curve *1*) and total internal reflection angle (curve *2*).

$H_\ell^{(1)}(q) = J_\ell(q) + i\, N_\ell(q)$, where $J_\ell(q)$ is a Bessel function and $N_\ell(q)$ is a Neumann function:

$$E_r^{(s)} = -\frac{1}{k_m r} \sum_{\ell=-\infty}^{\infty} (-i)^\ell \ell a_\ell H_\ell^{(1)}(k_m r) e^{i\ell\varphi}, \tag{8}$$

$$E_\varphi^{(s)} = -i \sum_{\ell=-\infty}^{\infty} (-i)^\ell a_\ell H_\ell^{(1)\prime}(k_m r) e^{i\ell\varphi}, \tag{9}$$

$$H_z^{(s)} = -i \sum_{\ell=-\infty}^{\infty} (-i)^\ell a_\ell H_\ell^{(1)}(k_m r) e^{i\ell\varphi}. \tag{10}$$

The fields inside the cylinder, denoted by the superscript t, are given by the formulas

$$E_r^{(t)} = \frac{1}{k_p r} \sum_{\ell=-\infty}^{\infty} (-1)^\ell \ell b_\ell J_\ell(k_p r) e^{i\ell\varphi}, \tag{11}$$

$$E_\varphi^{(t)} = i \sum_{\ell=-\infty}^{\infty} (-1)^\ell \ell b_\ell J_\ell'(k_p r) e^{i\ell\varphi}, \tag{12}$$

$$H_z = -n \sum_{\ell=-\infty}^{\infty} (-1)^\ell b_\ell J_\ell(k_p r) e^{i\ell\varphi}. \tag{13}$$

Here, $k_{m,p}$ are the wave vectors in the external medium (subscript m) and in the particle (subscript p); the factors a_ℓ and b_ℓ are the amplitudes of the corresponding modes, which are defined as

$$a_\ell = \frac{n J_\ell(nq) J_\ell'(q) - J_\ell'(nq) J_\ell(q)}{n J_\ell(nq) H_\ell^{(1)\prime}(q) - J_\ell'(nq) H_\ell^{(1)}(q)}, \tag{14}$$

$$b_\ell = \frac{J_\ell(q) H_\ell^{(1)\prime}(q) - J_\ell'(q) H_\ell^{(1)}(q)}{n J_\ell(nq) H_\ell^{(1)\prime}(q) - J_\ell'(nq) H_\ell^{(1)}(q)}. \tag{15}$$

Here, q is the size parameter; the prime means differentiation, i.e., $J_\ell'(z) = dJ_\ell(z)/dz$. These formulas are applicable for cylinders of arbitrary sizes, both metal [73] and dielectric ones.

Figure 15a shows the intensity distribution $I = |\mathbf{E}|^2$ in the cross section of a cylinder with a refractive index $n = 1.5$ and a size parameter $q = 10$. This is a typical pattern for field distribution in a photonic jet [6]. As direct numerical calculations show [61], small truncations of the cylinder (see Fig. 14c) do not affect qualitatively this pattern.

The main changes in the field in the resonance domain are related to the changes in the field inside the cylinder. For light incident at a total internal reflection angle $\chi_0 = \arcsin(n_m/n_p)$, the flat surface ab plays the role of a mirror. Resonance occurs when a ray, being reflected several times from the spherical surface, returns to the initial position (see Fig. 15b). Obviously, due to the multiple transmissions, the intensity of this "resonant ray" exceeds that of the rays propagating at other angles. For a spherical particle the first resonance is observed at $\chi = 45°$. For small truncations the value of this resonant angle χ depends on h and is determined from the equation

$$(1-h)\cos\chi + \sqrt{(1-h)^2 \cos^2\chi + h(2-h)}$$
$$\times \left(\cos\chi + \sin\chi \cot\left[\frac{\pi-\chi}{3}\right]\right) = 2-h. \tag{16}$$

The first and second terms on the left-hand side of (16) are the projections of the segments BS and AB, respectively, on the abscissa axis. In sum these projections make the segment AC. In Fig. 15c $\chi(h) \simeq \pi/4$ (Fig. 15c, red curve *1*). Due to the distortion of the ray path in the truncated cylinder, the bright "diamond" (see Fig. 14b) is distorted along the AC direction, and the specular reflection angle at the resonance becomes larger than 45°. In the case presented in Fig. 15b it amounts to about 46°.

A wave phase jump occurs at the intersection of the flat surface of Janus particle with the cylindrical or

spherical surface. In this case the classical Snell law of refraction is replaced with the generalized refraction law, which considers the influence of the phase gradient $d\Phi/dx$ [74]:

$$n_p \sin\theta_p - n_m \sin\theta_m = \frac{\lambda}{2\pi}\frac{d\Phi}{dx}. \tag{17}$$

According to the generalized refraction law, the total internal reflection angle changes:

$$\chi = \arcsin\left(\frac{n_m}{n_p} + \frac{\lambda}{2\pi n_p}\frac{d\Phi}{dx}\right). \tag{18}$$

The phase gradient can be estimated in the geometric optics approximation. The phase of the cut-off element is $\Delta\Phi = n_m 2\pi h/\lambda$. This accumulated phase difference arises at a distance of $\Delta x = \sqrt{(2-h)h}$, a half-length of segment ab (see Fig. 15b). As a result, formula (18) takes the form

$$\chi \approx \arcsin\left[\frac{n_m}{n_p}\left(1 + \sqrt{\frac{h}{2(n_p^2 - 1)}}\right)\right]. \tag{19}$$

According to this formula, the χ value is close to $\pi/4$ even at $h \approx 0.01$, which is consistent with the results of the numerical calculations presented in Fig. 15c. In this case formula (19) gives a value practically coinciding with the result of the numerical solution.

The interference of the waves incident on a flat surface at total internal reflection angles, forms high-intensity evanescent fields near the surface (see Figs. 14d, 15b). These fields were used previously to perform surface nanostructuring [75]. To implement this interference, the length of the segment Δx should exceed λ. This yields a limitation on the size parameter: $q > 2\pi/\sqrt{h} \gg 1$. More exact values can be obtained by solving numerically the Maxwell equations for a Janus particle.

Thus, Janus particles subjected to small truncations make it possible to excite surface electromagnetic waves on a localized area of a flat surface. This method is competitive with the interference method, which involves bound states in the continuum.

5. CONCLUSIONS

Recently a number of new optical effects have been discovered for dielectric mesoscale particles with $q \sim 10$ [50, 76]. These effects include optical and magnetic nanojets [6] and other effects, considered previously in review [50] for spherical particles. The emphasis of this review is on microscopic lenses providing super-resolved virtual images [5, 11, 12] and Janus particles with a small truncation [61]. These effects have a number of promising applications, some of which were discussed in [4, 5, 32, 58].

CONFLICT OF INTEREST

The authors declare that they have no conflicts of interest.

REFERENCES

1. *History of Optics* (Wikipedia). https://en.wikipedia.org/wiki/History_of_optics

2. M. N. Libenson, "Overcoming the diffractive limit in optics," *Soros Obrazovat. Zh.* **6** (3), 99−104 (2000) [in Russian].

3. Z. B. Wang and B. Luk'yanchuk, "Super-resolution imaging and microscopy by dielectric particle-lenses," in *Label-Free Super-Resolution Microscopy. Biological and Medical Physics, Biomedical Engineering*, Ed. by V. Astratov (Springer, Cham, 2019), pp. 371−400. https://doi.org/10.1007/978-3-030-21722-8_15

4. Z. B. Wang, B. Luk'yanchuk, L. Yue, B. Yan, J. Monks, R. Dhama, O. V. Minin, I. V. Minin, S. M. Huang, and A. A. Fedyanin, "High order Fano resonances and giant magnetic fields in dielectric microspheres," *Sci. Rep.* **9**, 20293 (2019). https://doi.org/10.1038/s41598-019-56783-3

5. Z. Wang, W. Guo, L. Li, B. Luk'yanchuk, A. Khan, Z. Liu, Z. Chen, and M. Hong, "Optical virtual imaging at 50 nm lateral resolution with a white-light nanoscope," *Nat. Commun.* **2**, 218 (2011). https://doi.org/10.1038/ncomms1211

6. B. S. Luk'yanchuk, R. Paniagua-Domınguez, I. V. Minin, O. V. Minin, and Z. B. Wang, "Refractive index less than two: Photonic nanojets yesterday, today and tomorrow," *Opt. Mater. Express* **7** (6), 1820−1847 (2017). https://doi.org/10.1364/OME.7.001820

7. H. Wang, C. J. R. Sheppard, K. Ravi, S. T. Ho, and G. Vienne, "Fighting against diffraction: Apodization and near field diffraction structures," *Laser Photonics Rev.* **6** (3), 354−392 (2012). https://doi.org/10.1002/lpor.201100009

8. H. Cang, A. Salandrino, Y. Wang, and X. Zhang, "Adiabatic far-field sub-diffraction imaging," *Nat. Commun.* **6**, 7942 (2015). https://doi.org/10.1038/ncomms8942

9. C. Simovsky and R. Heydarian, "A simple glass microsphere may put the end to the metamaterial superlens

story," *AIP Conf. Proc.* **2300**, 020117 (2020).
https://doi.org/10.1063/5.0031707

10. J. Kofler and N. Arnold, "Axially symmetric focusing as a cuspoid diffraction catastrophe: Scalar and vector cases and comparison with the theory of Mie," *Phys. Rev. B* **73** (23), 235401 (2006).
https://doi.org/10.1103/PhysRevB.73.235401

11. A. R. Bekirov, B. S. Luk'yanchuk, and A. A. Fedyanin, "Virtual image within a transparent dielectric sphere," *JETP Lett.* **112**, 341−345 (2020).
https://doi.org/10.1134/S0021364020180058

12. A. R. Bekirov, B. S. Luk'yanchuk, Z. Wang, and A. A. Fedyanin, "Wave theory of virtual image [Invited]," *Opt. Mater. Express* **11**, 3646−3655 (2021).
https://doi.org/10.1364/OME.437467

13. C. F. Bohren and D. R. Huffman, *Absorption and Scattering of Light by Small Particles* (Wiley−Interscience, New York, 2004).
https://doi.org/10.1002/9783527618156

14. P. W. Barber and S. C. Hill, *Light Scattering by Particles: Computational Methods* (World Sci., Singapore, 1990).
https://doi.org/10.1142/0784

15. Y. Duan, G. Barbastathis, and B. Zhang, "Classical imaging theory of a microlens with super-resolution," *Opt. Lett.* **38** (16), 2988−2990 (2013).
https://doi.org/10.1364/OL.38.002988

16. A. Darafsheh, G. F. Walsh, L. Dal Negro, and V. N. Astratov, "Optical super-resolution by high-index liquid immersed microspheres," *Appl. Phys. Lett.* **101**, 141128 (2012).
https://doi.org/10.1063/1.4757600

17. S. Lee, L. Li, Y. Ben-Aryeh, Z. Wan, and W. Guo, "Overcoming the diffraction limit induced by microsphere optical nanoscopy," *J. Opt.* **15** (12), 125710 (2013).
https://doi.org/10.1088/2040-8978/15/12/125710

18. L. A. Krivitsky, J. J. Wang, Z. Wang, and B. Luk'yanchuk, "Locomotion of microspheres for super-resolution imaging," *Sci. Rep.* **3**, 3501 (2013).
https://doi.org/10.1038/srep03501

19. A. Darafsheh, N. I. Limberopoulos, J. S. Derov, D. E. Walker, Jr., and V. N. Astratov, "Advantages of microsphere assisted super-resolution imaging technique over solid immersion lens and confocal microscopies," *Appl. Phys. Lett.* **104**, 061117 (2014).
https://doi.org/10.1063/1.4864760

20. L. Martin-Moreno, F. J. Garcia-Vidal, H. J. Lezec, K. M. Pellerin, T. Thio, J. B. Pendry, and T. W. Ebbesen, "Theory of extraordinary optical transmission through subwavelength hole arrays," *Phys. Rev. Lett.* **86**, 1114−1117 (2001).
https://doi.org/10.1103/PhysRevLett.86.1114

21. C. Genet and T. W. Ebbesen, "Light in tiny holes," *Nature* **445**, 39−46 (2007).
https://doi.org/10.1038/nature05350

22. F. J. Garcia-Vidal, L. Martin-Moreno, T. W. Ebbesen, and L. Kuipers, "Light passing through subwavelength apertures," *Rev. Mod. Phys.* **82**, 729−787 (2010).
https://doi.org/10.1103/RevModPhys.82.729

23. Y. Xie, A. R. Zakharian, J. V. Moloney, and M. Mansuripur, "Transmission of light through slit apertures in metallic films," *Opt. Express* **12**, 6106−6121 (2004).
https://doi.org/10.1364/OPEX.12.006106

24. B. S. Luk'yanchuk, Y. W. Zheng, and Y. F. Lu, "Laser cleaning of solid surface: optical resonance and near-field effects," *Proc. SPIE* **4065**, 576−587 (2000).
https://doi.org/10.1117/12.407350

25. P. A. Bobbert and J. Vlieger, "Light scattering by a sphere on a substrate," *Physica A* **137** (1-2), 209−242 (1986).
https://doi.org/10.1016/0378-4371(86)90072-5

26. V. M. Sundaram and S. B. Wen, "Analysis of deep sub-micron resolution in microsphere-based imaging," *Appl. Phys. Lett.* **105**, 204102 (2014).
https://doi.org/10.1063/1.4902247

27. B. R. Johnson, "Light scattering from a spherical particle on a conducting plane: I. Normal incidence: Errata," *J. Opt. Soc. Am. A* **10**, 766 (1993). https://opgica.org/josaa/abstract.cfm?uri=josaa-10-4-766
https://doi.org/10.1364/JOSAA.10.000766

28. M. X. Wu, B. J. Huang, R. Chen, Y. Yang, J. F. Wu, R. Ji, X. D. Chen, and M. H. Hong, "Modulation of photonic nanojets generated by microspheres decorated with concentric rings," *Opt. Express* **23**, 20096−20103 (2015).
https://doi.org/10.1364/OE.23.020096

29. E. Narimanov, "Resolution limit of label-free far-field microscopy," *Adv. Photonics* **1**, 056003 (2019).
https://doi.org/10.1117/1.AP.1.5.056003

30. N. I. Zheludev and G. Yuan, "Optical superoscillation technologies beyond the diffraction limit," *Nat. Rev. Phys.* **4**, 16-32 (2022).
https://doi.org/10.1038/s42254-021-00382-7

31. G. H. Yuan and N. I. Zheludev, "Detecting nanometric displacements with optical ruler metrology," *Science* **364**, 771−775 (2019).
https://doi.org/10.1126/science.aaw7840

32. Z. Wang, B. Luk'yanchuk, and L. Wu, "Roadmap for label-free imaging with microsphere superlens and metamaterial solid immersion lens," arXiv:2108.09153 (2021).

33. *Label-Free Super-Resolution Microscopy*, Ed. by V. Astratov (Springer, Cham, 2019).
https://doi.org/10.1007/978-3-030-21722-8

34. A. Darafsheh, "Microsphere-assisted microscopy," *J. Appl. Phys.* **131**, 031102 (2022).
https://doi.org/10.1063/5.0068263

35. J. W. Strutt (Lord Rayleigh), "Investigations in optics, with spectral reference to the spectroscope," *Philos. Mag. Ser. 5*, **8** (49) (1879).
https://doi.org/10.1080/14786447908639684

36. D. W. Pohl, W. Denk, and M. Lanz, "Optical stethoscopy: Image recording with resolution $\lambda/20$," *Appl. Phys. Lett.* **44**, 651−653 (1984).
https://doi.org/10.1063/1.94865

37. V. G. Veselago, "The electrodynamics of substances with simultaneously negative values of ε and μ," *Sov. Phys.-Usp.* **10** (4), 509−514 (1968).
https://doi.org/10.1070/PU1968v010n04ABEH003699

38. J. B. Pendry, "Negative refraction makes a perfect lens," *Phys. Rev. Lett.* **85** (18), 3966−3969 (2000).
https://doi.org/10.1103/PhysRevLett.85.3966

39. S. W. Hell and J. Wichmann, "Breaking the diffraction resolution limit by stimulated emission: Stimulated-emission-depletion fluorescence microscopy," *Opt.*

Lett. **19**, 780−782 (1994).
https://doi.org/10.1364/OL.19.000780

40. B. Huang, M. Bates, and X. Zhuang, "Super-resolution fluorescence microscopy," *Annu. Rev. Biochem.* **78**, 993−1016 (2009).
https://doi.org/10.1146/annurev.biochem.77.061906.092014

41. E. T. Rogers, J. Lindberg, T. Roy, S. Savo, J. E. Chad, M. R. Dennis, and N. I. Zheludev, "A super-oscillatory lens optical microscope for subwavelength imaging," *Nat. Mater.* **11**, 432−435 (2012).
https://doi.org/10.1038/nmat3280

42. P. Davidovits and M. D. Egger, "Scanning laser microscope for biological investigations," *Appl. Opt.* **10**, 1615−1619 (1971).
https://doi.org/10.1364/AO.10.001615

43. H. F. Wang, L. P. Shi, B. S. Luk'yanchuk, C. Sheppard, and T. C. Chong, "Creation of a needle of longitudinal polarized light in vacuum using binary optics," *Nat. Photonics* **2**, 501−505 (2008).
https://doi.org/10.1038/nphoton.2008.127

44. Q. Zhan, "Cylindrical vector beams: From mathematical concepts to applications," *Adv. Opt. Photonics* **1**, 1−57 (2009),
https://doi.org/10.1364/AOP.1.000001

45. R. Heydarian and C. Simovski, "Non-resonant subwavelength imaging by dielectric microparticles," *Photonics Nanostruct. Fundam. Appl.* **46**, 100950 (2021).
https://doi.org/10.1016/j.photonics.2021.100950

46. R. Heydarian and C. Simovski, "On subwavelength resolution granted by dielectric microparticles," arXiv:2203.01066 (March 2, 2022).

47. A. R. Bekirov, "Microsphere nanoscope and overcoming diffraction limit," *Proc. 13th International Conference and Expo on Nanotechnology & Nanomaterials* (Barcelona, Spain, July 12−14, 2021).

48. R. M. Bakker, Y. F. Yu, R. Paniagua-Domínguez, B. Luk'yanchuk, and A. I. Kuznetsov, "Resonant light guiding along a chain of silicon nanoparticles," *Nano Lett.* **17**, 3458−3464 (2017).
https://doi.org/10.1021/acs.nanolett.7b00381

49. M. Berry, N. Zheludev, Y. Aharonov, F. Colombo, I. Sabadini, D. C. Struppa, J. Tollaksen, E. T. Rogers, F. Qin, M. Hong, and X. Luo, "Roadmap on superoscillations," *J. Opt.* **21**, 053002 (2019).
https://doi.org/10.1088/2040-8986/ab0191

50. B. S. Luk'yanchuk, A. R. Bekirov, Z. B. Wang, I. V. Minin, O. V. Minin, and A. A. Fedyanin, "Optical phenomena in dielectric spheres several light wavelengths in size: A review," *Phys Wave Phenom.* **30** (4), 217−241 (2022).
https://doi.org/10.3103/S1541308X22040045

51. A. I. Kuznetsov, A. E. Miroshnichenko, Y. H. Fu, J. B. Zhang, and B. Luk'yanchuk, "Magnetic light," *Sci. Rep.* **2**, 492 (2012).
https://doi.org/10.1038/srep00492

52. L. Novotny and B. Hecht, *Principle of Nano-Optics* (Cambridge Univ. Press, Cambridge, 2012).
https://doi.org/10.1017/CBO9780511794193

53. W. Fan, B. Yan, Z. B. Wang, and L. M. Wu, "Three-dimensional all-dielectric metamaterial solid immersion lens for subwavelength imaging at visible frequencies,"

Sci. Adv. **2**, 1600901 (2016).
https://doi.org/10.1126/sciadv.1600901

54. Y. Shechtman, Y. C. Eldar, O. Cohen, H. N. Chapman, J. Miao, and M. Segev, "Phase retrieval with application to optical imaging: A contemporary overview," *IEEE Signal Process. Mag.* **32**, 87−109 (2015).
https://doi.org/10.1109/MSP.2014.2352673

55. A. Walther and A. H. E. Müller, "Janus particles," *Soft Matter* **4**, 663−668 (2008).
https://doi.org/10.1039/B718131K

56. J. Hu, S. Zhou, Y. Sun, X. Fanga, and L. Wu, "Fabrication, properties and applications of Janus particles," *Chem. Soc. Rev.* **41**, 4356−4378 (2012).
https://doi.org/10.1039/C2CS35032G

57. D. R. Mason, M. V. Jouravlev, and K. S. Kim, "Enhanced resolution beyond the Abbe diffraction limit with wavelength-scale solid immersion lenses," *Opt. Lett.* **35**, 2007−2009 (2010).
https://doi.org/10.1364/OL.35.002007

58. G. J. Lee, H. M. Kim, and Y. M. Song, "Design and fabrication of microscale, thin-film silicon solid immersion lenses for mid-infrared application," *Micromachines* **11**, 250 (2020).
https://doi.org/10.3390/mi11030250

59. I. Mahariq, I. Giden, H. Kurt, O. V. Minin, and I. V. Minin, "Strong electromagnetic field localization near the surface of hemicylindrical particles," *Opt. Quantum Electron.* **50**, 423 (2018).
https://doi.org/10.1007/s11082-017-1263-5

60. G. Gu, X. Shen, Z. Peng, X. Yang, S. Bandyopadhyay, J. Feng, D. Xiao, and L. Shao, "Numerical investigation of photonic nanojets generated from D-shaped dielectric microfibers," *Proc. SPIE* **11186**, 111861H (2019).
https://doi.org/10.1117/12.2538025

61. I. V. Minin, O. V. Minin, Y. Cao, B. Yan, Z. Wang, and B. Luk'yanchuk, "Photonic lenses with whispering gallery waves at Janus particles," *Opto-Electron. Sci.* **1**, 210008 (2022).
https://doi.org/10.29026/oes.2022.210008

62. G. S. Kino and S. M. Mansfield, US Patent 5,004,307 (1991).

63. A. S. Glassner, *An Introduction to Ray Tracing* (Academic, London, 1991). ISBN 0-12-286160-4.

64. L. P. Ghislain, V. B. Elings, K. B. Crozier, S. R. Manalis, S. C. Minne, K. Wilder, G. S. Kino, and C. F. Quate, "Near-field photolithography with a solid immersion lens," *Appl. Phys. Lett.* **74**, 501−503 (1999).
https://doi.org/10.1063/1.123168

65. M. Born and E. Wolf, *Principles of Optics: Electromagnetic Theory of Propagation, Interference, and Diffraction of Light* (Elsevier, Amsterdam, Netherlands, 2013).
https://doi.org/10.1017/CBO9781139644181

66. A. N. Oraevsky, "Whispering-gallery waves," *Quantum Electron.* **32**, 377−400 (2002).
https://doi.org/10.1070/QE2002v032n05ABEH002205

67. R. A. Yadav and I. D. Singh, "Normal modes and quality factors of spherical dielectric resonators: I—shielded dielectric sphere," *Pramana J. Phys.* **62**, 1255−1271 (2004).
https://doi.org/10.1007/BF02704438

68. H. Mabuchi, E. W. Streed, D. W. Vernooy, V. S. Ilchen-ko, and H. J. Kimble, "High-Q measurements of fused-silica microspheres in the near infrared," *Opt. Lett.* **23** (4), 247−249 (1998).
https://doi.org/10.1364/OL.23.000247

69. I. S. Grudinin, A. B. Matsko,A. A. Savchenkov, D. Strekalov, V. S. Ilchenko, and L. Maleki, "Ultra high Q crystalline microcavities," *Opt. Commun.* **265** (1), 33−38 (2006).
https://doi.org/10.1016/j.optcom.2006.03.028

70. M. V. Rybin, K. L. Koshelev, Z. F. Sadrieva, K. B. Samu-sev, A. A. Bogdanov, M. F. Limonov, and Y. S. Kivshar, "High-Q supercavity modes in subwavelength dielectric resonators," *Phys. Rev. Lett.* **119** (24), 243901 (2017).
https://doi.org/10.1103/PhysRevLett.119.243901

71. L. Carletti, K. Koshelev, C. De Angelis, and Y. Kivshar, "Giant nonlinear response at the nanoscale driven by bound states in the continuum," *Phys. Rev. Lett.* **121** (3), 033903 (2018).
https://doi.org/10.1103/PhysRevLett.121.033903

72. H. C. van de Hulst, *Light Scattering by Small Particles* (Dover, New York, 1981).
https://doi.org/10.1002/qj.49708436025

73. B. S. Luk'yanchuk, and V. Ternovsky, "Light scattering by thin wire with surface plasmon resonance: Bifurca-tions of the Poynting vector field," *Phys. Rev. B* **73** (23), 235432 (2006).
https://doi.org/10.1103/PhysRevB.73.235432

74. N. F. Yu, P. Genevet, M. A. Kats, F. Aieta, J. P. Teti-enne, F. Capasso, and Z. Gaburro, "Light propagation with phase discontinuities: Generalized laws of reflec-tion and refraction," *Science* **334**, 333−337 (2011).
https://doi.org/10.1126/science.1210713

75. Y. Zhou, M. H. Hong, J. Y. H. Fuh, L. Lu, and B. S. Lukiyanchuk, "Evanescent wave interference li-thography for surface nano-structuring," *Phys. Scr.* **2007** (T129), 35−37 (2007).
https://doi.org/10.1088/0031-8949/2007/T129/008

76. O. V. Minin and I. V. Minin, "Optical phenomena in mesoscale dielectric particles," *Photonics* **8**, 591 (2021).
https://doi.org/10.3390/photonics8120591

Translated by Yu. Sin'kov